PHOTONICS Research

Si/Si_3N_4/Ag hybrid nanocavity: a platform for enhancing light-matter interaction

Tianqi Peng,[1] Zhuo Wang,[1,*] Shulei Li,[2] Lidan Zhou,[3] Shimei Liu,[1] Yuheng Mao,[1] Mingcheng Panmai,[4] Weichen He,[5,6] and Sheng Lan[1]

[1]Guangdong Provincial Key Laboratory of Nanophotonic Functional Materials and Devices, School of Optoelectronic Science and Engineering, South China Normal University, Guangzhou 510006, China
[2]School of Optoelectronic Engineering, Guangdong Polytechnic Normal University, Guangzhou 510665, China
[3]State Key Laboratory of Optoelectronic Materials and Technologies, School of Electronics and Information Technology, Sun Yat-sen University, Guangzhou 510006, China
[4]School of Electrical and Electronic Engineering, Nanyang Technological University, Singapore 639798, Singapore
[5]GBA Branch of Aerospace Information Research Institute, Chinese Academy of Sciences, Guangzhou 510700, China
[6]Guangdong Provincial Key Laboratory of Terahertz Quantum Electromagnetics, Guangzhou 510700, China
*Corresponding author: zhuowang@m.scnu.edu.cn

Received 9 August 2024; revised 27 December 2024; accepted 10 January 2025; posted 10 January 2025 (Doc. ID 538704); published 28 February 2025

High-index dielectric nanoparticles supporting strong Mie resonances, such as silicon (Si) nanoparticles, provide a platform for manipulating optical fields at the subwavelength scale. However, in general, the quality factors of Mie resonances supported by an isolated nanoparticle are not sufficient for realizing strong light-matter interaction. Here, we propose the use of dielectric-metal hybrid nanocavities composed of Si nanoparticles and silicon nitride/silver (Si_3N_4/Ag) heterostructures to improve light-matter interaction. First, we demonstrate that the nonlinear optical absorption of the Si nanoparticle in a Si/Si_3N_4/Ag hybrid nanocavity can be greatly enhanced at the magnetic dipole resonance. The Si/Si_3N_4/Ag nanocavity exhibits luminescence burst at substantially lower excitation energy (~20.5 pJ) compared to a Si nanoparticle placed on a silica substrate (~51.3 pJ). The luminescence intensity is also enhanced by an order of magnitude. Second, we show that strong exciton-photon coupling can be realized when a tungsten disulfide (WS_2) monolayer is inserted into a Si/Si_3N_4/Ag nanocavity. When such a system is excited by using s-polarized light, the optical resonance supported by the nanocavity can be continuously tuned to sweep across the two exciton resonances of the WS_2 monolayer by simply varying the incident angle. As a result, Rabi splitting energies as large as ~146.4 meV and ~110 meV are observed at the A- and B-exciton resonances of the WS_2 monolayer, satisfying the criterion for strong exciton-photon coupling. The proposed nanocavities provide, to our knowledge, a new platform for enhancing light-matter interaction in multiple scenarios and imply potential applications in constructing nanoscale photonic devices.

https://doi.org/10.1364/PRJ.538704

1. INTRODUCTION

High-index dielectric nanoparticles supporting distinct Mie resonances have aroused widespread research interest due to their excellent light manipulation performance at the subwavelength scale [1]. In 2010, resonance-enhanced light scattering from silicon (Si) nanowires was first observed in the visible and near-infrared spectral range [2,3]. Since then, the research on strong electric and magnetic responses and their interactions in high-index nanoparticles has revealed rich resonance-induced phenomena including structural color [4–6], directional scattering [7–10], scattering suppression by an anapole mode [11], significant enhancement of nonlinear optical response [12,13], and so on. Compared with metallic nanoparticles, dielectric nanoparticles support magnetic resonances and possess much lower optical loss. These advantages lead to the strongly localized electric field inside dielectric nanoparticles at optical resonances, greatly improving light-matter interaction.

Increasing quality factors (Q factors) of resonant modes is vital for generating remarkable near-field enhancement [14–16] and achieving strong light-matter interaction [17]. In 2012, it was found that a dielectric nanoparticle placed on a gold (Au) substrate can interact strongly with its mirror image [18]. A further study revealed that the cooperation of the electric dipole (ED) excited in the nanoparticle and its virtual counterpart can be interpreted as a mirror-image-induced magnetic dipole (MMD), leading to enhanced scattering [19]. In

addition, the Q factor of the magnetic dipole (MD) resonance supported by the Si/Au nanocavity can be effectively improved by optimizing the polarization and angle of the incident light [20]. For a nanocavity composed of a Si nanoparticle, a silica (SiO_2) spacer, and a silver (Ag) substrate, the resonant strength and linewidth of the ED and MD modes can be manipulated by varying the thickness of the spacer layer. It was demonstrated that the thin SiO_2 spacer greatly enhanced the MD resonance in the Si nanoparticle and induced phonon-assisted hot luminescence [21]. Besides, when metals are introduced into a system, it is important to reduce Ohmic loss [22]. The SiO_2 spacer separates the Si nanoparticle from the Ag substrate, which effectively suppresses the effect of Ohmic loss on the optical modes in the Si nanoparticle. Therefore, a nanocavity composed of a high-index nanoparticle and a dielectric-metal heterostructure acts as a good platform for realizing the enhancement of light-matter interaction at the subwavelength scale.

As the core material for optoelectric devices, Si has excellent characteristics of high refractive index and low material loss in the visible and near-infrared bands. Light emitters based on Si nanostructures have always attracted particular interest as they provide unique opportunities for highly integrated light sources for photonic circuits [23]. An on-chip Si light source could potentially achieve a higher integration density with a compact size and display better performance in terms of energy efficiency [24]. However, the quantum efficiency of bulk Si is limited by indirect bandgap structure [25]. Hence, resonance-enhanced light-matter interaction is essential to improve the luminescence performance of Si nanoparticles or nanostructures. In 2018, white light emission from Si nanoparticles placed on a SiO_2 substrate was demonstrated by resonantly exciting their MD resonances with femtosecond laser pulses [26]. The luminescence is caused by the interband transition of hot carriers enhanced by the Auger effect and Purcell effect, which is different from that caused by the intraband transition of hot carriers in GaAs [27]. The efficiency of the white light emission was further enhanced by improving the Q factor of the resonant mode at the excitation wavelength, for example, adopting the MMD resonance of a Si nanoparticle placed on a metal substrate [28] or quasi-bound states in the continuum of a Si nano cuboid [29] and a Si metasurface [30]. These strategies can substantially reduce the threshold for the luminescence burst. In addition, it was reported that the MD resonance of a Si nanoparticle can be effectively enhanced by adding a SiO_2 spacer in between the nanoparticle and an Ag substrate [21]. Although it has been known that the optical modes supported by a Si nanoparticle can be modified by a dielectric-metal heterostructure, a systematic study on the linear and nonlinear optical properties of a hybrid nanocavity composed of a Si nanoparticle and a dielectric-metal heterostructure is still lacking.

Mie resonances with high Q factors can not only enhance the interaction between the optical mode and the cavity itself but also enhance the interaction between light and two-dimensional (2D) materials. A dielectric-metal heterostructure can support transverse-electric-polarized (TE-polarized) surface-bound waves [31] under the physical mechanism of optical magnetism [32]. The TE wave, which is dominated by the in-plane electric field, can fully interact with 2D material embedded into the heterostructure. For example, a narrow linewidth TE wave supported by a silicon nitride/silver (Si_3N_4/Ag) heterostructure can interact with a tungsten disulfide (WS_2) monolayer to achieve strong exciton-photon coupling [33]. However, being a surface-bound wave, the confinement of the electromagnetic field in the propagation direction of the TE wave is still lacking. Therefore, it is necessary to introduce a high-index dielectric nanoparticle on the surface of the Si_3N_4/Ag heterostructure to improve local field enhancement for further enhancing light-matter interaction.

In this paper, we investigate systematically the enhanced light-matter interaction based on Si/Si_3N_4/Ag hybrid nanocavities. Both low-threshold luminescence burst and strong exciton-photon coupling are demonstrated. First, the enhanced MD resonance in the Si/Si_3N_4/Ag hybrid nanocavity substantially improves the nonlinear-optical-absorption-induced interband transition of hot electrons. With the help of the Auger effect [34] and Purcell effect, luminescence burst from the Si/Si_3N_4/Ag nanocavity is stimulated by femtosecond laser pulses with low energy of ~20.5 pJ. Compared with the case of a Si nanoparticle placed on a SiO_2 substrate, not only the threshold pulse energy is reduced by 30.8 pJ, but also the luminescence intensity is increased by one order of magnitude. Second, a WS_2 monolayer is placed in between the Si nanoparticle and Si_3N_4/Ag heterostructure to achieve strong exciton-photon coupling with the excitation of s-polarized light. By changing the incident angle of s-polarized light, the resonant wavelength of the optical mode can be adjusted covering the two exciton resonances of the WS_2 monolayer. Large Rabi splitting energies of ~146.4 meV and ~110 meV are obtained at the A- and B-exciton (X_A and X_B) resonances, respectively.

2. RESULTS AND DISCUSSION

We first examine the effect of a Si_3N_4/Ag heterostructure on the Mie resonances of a Si nanoparticle based on numerical simulation. As schematically shown in Fig. 1(a), a Si nanoparticle with a diameter of d is placed on a Si_3N_4/Ag/SiO_2 substrate. The thicknesses of the Ag film and Si_3N_4 spacer are noted as h_1 and h_2, respectively. The Si nanoparticle is illuminated by a broadband light source propagating along the $-z$ direction and the backward scattering is collected by an objective. We performed the simulation with the commercial software Ansys Lumerical based on the finite-difference time-domain (FDTD) method. In Fig. 1(b), we show the evolution of the scattering spectrum of a Si/Si_3N_4/Ag nanocavity ($d = 195$ nm) when the thickness of the Ag film is fixed ($h_1 = 50$ nm) and that of the Si_3N_4 spacer layer is increased. It is noticed that the intensity of the optical resonance located at ~765 nm is enhanced significantly when h_2 is in the range from 70 to 95 nm. In addition, it is found that the intensity of the optical resonance located around 600 nm begins to increase when h_2 rises beyond 95 nm. These behaviors imply that the optical resonances supported by the Si/Si_3N_4/Ag nanocavity can be effectively manipulated by simply varying the thickness of the Si_3N_4 spacer layer. Based on multipolar decomposition (see Appendix A), we reveal that the optical resonances appearing around 600 nm and 765 nm are dominated by ED and MD, respectively. The scattering spectra of the

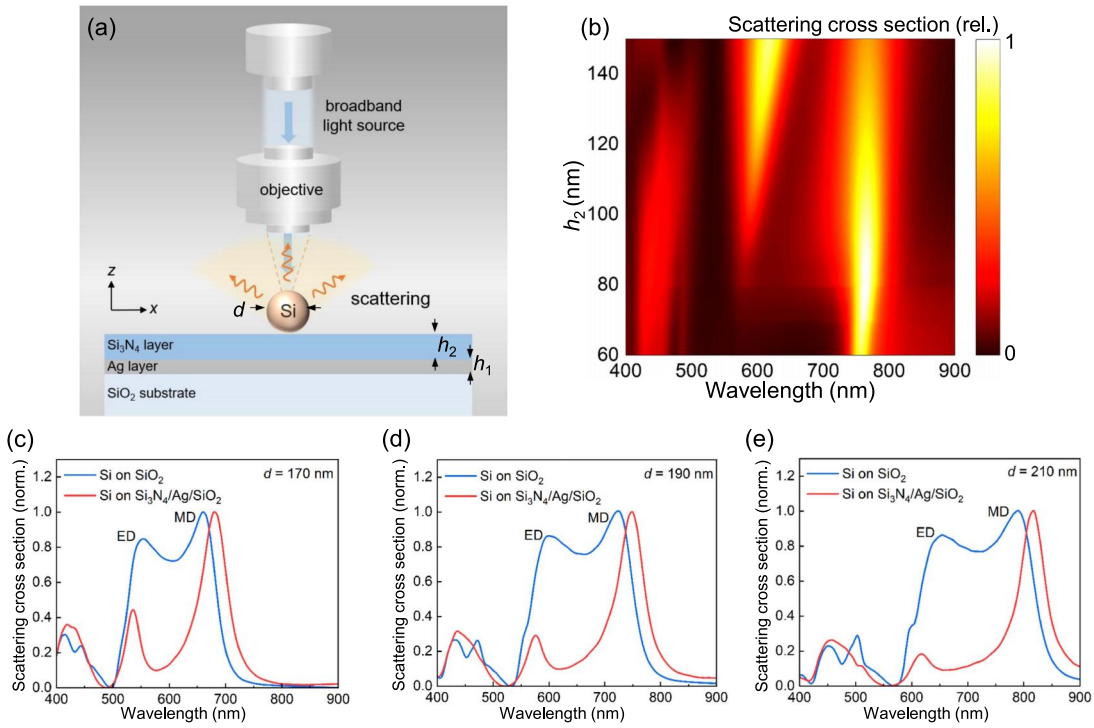

Fig. 1. Optical resonances supported by a $Si/Si_3N_4/Ag$ nanocavity. (a) Schematic configuration of a $Si/Si_3N_4/Ag$ hybrid nanocavity. (b) Calculated scattering spectra (normalized to the maximum value) of $Si/Si_3N_4/Ag$ nanocavities ($d = 195$ nm, $h_1 = 50$ nm) with variable Si_3N_4 spacer layer thickness. (c)–(e) Comparison of the scattering spectra (each spectrum is normalized to its maximum value) of Si nanoparticles with different diameters placed on a $Si_3N_4/Ag/SiO_2$ substrate ($h_1 = 50$ nm, $h_2 = 95$ nm) (red curves) and a SiO_2 substrate (blue curves).

nanocavity with different h_1 are discussed in Appendix B, which indicates that a 50 nm Ag layer is sufficient to be a good reflector. We examined the effects of a Si_3N_4/Ag heterostructure ($h_1 = 50$ nm, $h_2 = 95$ nm) on the scattering properties of a Si nanoparticle. As shown in Figs. 1(c)–1(e), we compared the scattering spectra of Si nanoparticles with different diameters on a SiO_2 substrate with and without the Si_3N_4/Ag heterostructure. The results reveal that increasing the diameter of the Si nanoparticle primarily increases the resonant wavelengths of both ED and MD resonances. In addition, it is noticed that the Q factors of the ED and MD resonances are improved by using the Si_3N_4/Ag heterostructure. The Q factors of the ED and MD resonant modes can be calculated by the formula $Q = \lambda/\Delta\lambda$, where λ is the peak wavelength in the scattering spectrum of each mode and $\Delta\lambda$ is the full width at half maximum (FWHM) of the scattering spectrum. Gaussian fitting functions were used to extract $\Delta\lambda$ of each resonant mode from the scattering spectrum. Without loss of generality, taking the result in Fig. 1(d) as an example, the Q factors of ED and MD increase from 7.2 and 8.2 to 18.6 and 11.4, respectively, after the introduction of the Si_3N_4/Ag heterostructure. The improvement of Q factor results from the destructive interference of the in-plane ED or MD with its mirror mode reflected from the Ag film. Here the Si_3N_4/Ag heterostructure acts as a Fabry–Perot cavity. The degree of interference cancellation of the out-of-plane radiation can be tuned by varying the thickness of the spacer [16,35].

The energy band structure of Si and the carrier dynamics in a Si nanoparticle excited by femtosecond laser pulses are depicted schematically in Fig. 2(a). Since the energy gap between the conduction and valence bands at the Γ point is 3.4 eV, the interband transition of electrons is initiated by two- or three-photon-induced absorption (2PA or 3PA) of femtosecond laser pulses. The enhancement factors of 2PA and 3PA (I^2 and I^3) are proportional to the fourth and sixth power of the electric field inside the Si nanoparticle, respectively, i.e., $I^2 = (1/V)\int_{Si}(|E|/|E_0|)^4 dV$, $I^3 = (1/V)\int_{Si}(|E|/|E_0|)^6 dV$, where $E_0 = 1$ is the amplitude of the incident electric field and V is the volume of the Si nanoparticle. Therefore, it is expected that the 2PA and 3PA of a Si nanoparticle will be effectively enhanced at the ED and MD resonances, generating high-density carriers in the Si nanoparticle. Owing to the Auger effect, the non-radiative recombination lifetime (τ_{nr}) of hot electrons can be significantly increased (from 0.1–1.0 ps to 10–100 ps). Theoretically, the fluorescence quantum efficiency (η) of a Si nanoparticle can be described by the formula $\eta = 1/(1 + \tau_r/\tau_{nr})$, where τ_r represents the radiative recombination lifetime of hot electrons at the emission wavelength. Relying on the Purcell effect, the radiative recombination lifetime can be reduced by exploiting the high-order Mie resonances of the Si nanoparticle, such as the electric quadrupole (EQ) and magnetic quadrupole (MQ) resonances. Therefore, the combination of the Auger effect and the Purcell effect can dramatically enhance the nonlinear photoluminescence (PL) of a Si nanoparticle.

Figure 2(b) illustrates the scattering and 2PA/3PA spectra calculated for the $Si/Si_3N_4/Ag$ hybrid nanocavity

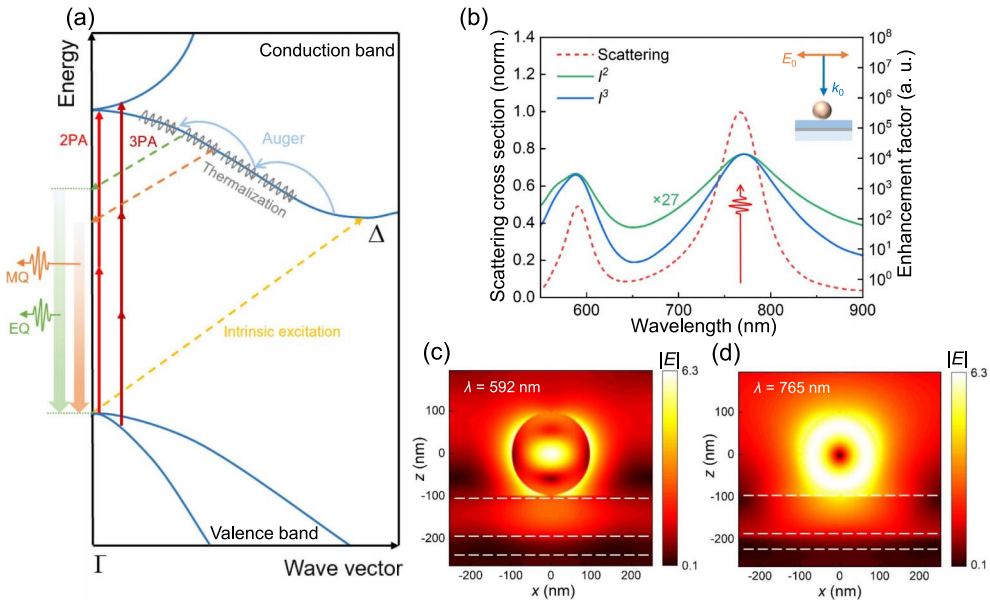

Fig. 2. Physical mechanism for the enhanced nonlinear optical emission from a $Si/Si_3N_4/Ag$ nanocavity. (a) Energy band diagram of Si and carrier dynamics in a Si nanoparticle excited by femtosecond laser pulses. (b) Calculated scattering and 2PA/3PA spectra for a Si nanoparticle ($d = 195$ nm) placed on a $Si_3N_4/Ag/SiO_2$ substrate. The scattering spectrum is normalized to its maximum value. (c), (d) Electric field amplitude distributions in the $Si/Si_3N_4/Ag$ hybrid nanocavity calculated at the ED and MD resonances.

($d = 195$ nm, $h_1 = 50$ nm, $h_2 = 95$ nm). One can see that the enhancement factors of 2PA and 3PA reach peak values at the ED (~592 nm) and MD (~765 nm) resonances of the $Si/Si_3N_4/Ag$ nanocavity. The electric field distributions at the ED and MD resonances are shown in Figs. 2(c) and 2(d), respectively. Remarkably, the electric field is strongly localized in the Si nanoparticle at the MD resonance, leading to larger enhancement factors of 2PA and 3PA than those at the ED resonance. Compared with the Si nanoparticle placed on a SiO_2 substrate (see Appendix C), the enhancement factors of 2PA and 3PA are improved by ~21 and ~95 times, respectively.

We studied the nonlinear optical emission of a $Si/Si_3N_4/Ag$ hybrid nanocavity ($d \sim 190$ nm, $h_1 \sim 50$ nm, $h_2 \sim 95$ nm) under the excitation of femtosecond laser pulses. The detailed experimental setup is described in Appendix D. In Fig. 3(a), we show the evolution of the PL spectrum of the $Si/Si_3N_4/Ag$ nanocavity with increasing pumping energy. The excitation wavelength was set at the MD resonance of the nanocavity (~750 nm) based on the scattering spectrum shown in Fig. 3(b). In each case, the emission from the nanocavity was recorded by using a charge-coupled device (CCD), as shown in the insets of Fig. 3(a). When the pulse energy was increased from 3.9 to 15.8 pJ, the hot electron luminescence from the nanocavity increased only slightly. Notably, a burst of white light emission from the nanocavity was observed when the pulse energy exceeded 20.5 pJ. The cooperation of the intrinsic excitation and the Auger effect leads to a large number of hot electrons in the high-energy states (around the Γ point), which significantly enhances the nonlinear optical emission. In Fig. 3(b), we compared the scattering spectra of the nanocavity before and after the luminescence burst. It is noticed that the scattering intensities of the nanocavity at the MD and ED resonances are greatly enhanced after the luminescence burst. This phenomenon can be ascribed to the annealing of the Si nanoparticle by the high temperature induced by the laser pulses, improving the quality of the crystalline structure. In addition, the scattering peaks of MD and ED are blue-shifted and red-shifted, respectively. It is caused by the giant optical force applied by femtosecond laser pulses on the Si nanoparticle. Under the optical force, the nanoparticle is squeezed in the out-of-plane direction and stretched in the plane along the polarization direction of the incident light [36]. In addition, the MQ resonance at ~560 nm is excited by the large-angle components of the broadband incident light focused by using an objective with a numerical aperture (NA) of 0.8 (see Appendix A). In Fig. 3(c), we present the dependence of the integrated PL intensity on the excitation pulse energy observed for the nanocavity. It can be seen that the PL intensity increases exponentially when the excitation pulse energy exceeds 20.5 pJ. For comparison, we also examined the nonlinear optical emission of a Si nanoparticle placed on a SiO_2 substrate. Based on the scattering spectra shown in Fig. 3(e), the excitation wavelength was chosen at 745 nm so that the MD resonance was resonantly excited. As shown in Fig. 3(d), the luminescence burst could be observed only when the excitation pulse energy was raised to 51.3 pJ. This behavior is also shown in Fig. 3(f) where the dependence of the integrated PL intensity on the pumping pulse energy is presented. By comparing the results shown in Figs. 3(c) and 3(f), it can be seen that the threshold for the luminescence burst is greatly reduced in the $Si/Si_3N_4/Ag$ nanocavity when the Si_3N_4/Ag heterostructure is used as the substrate. More importantly, it is found that the PL intensity of the $Si/Si_3N_4/Ag$ nanocavity is one order of magnitude larger than that of the Si nanoparticle on the SiO_2 substrate.

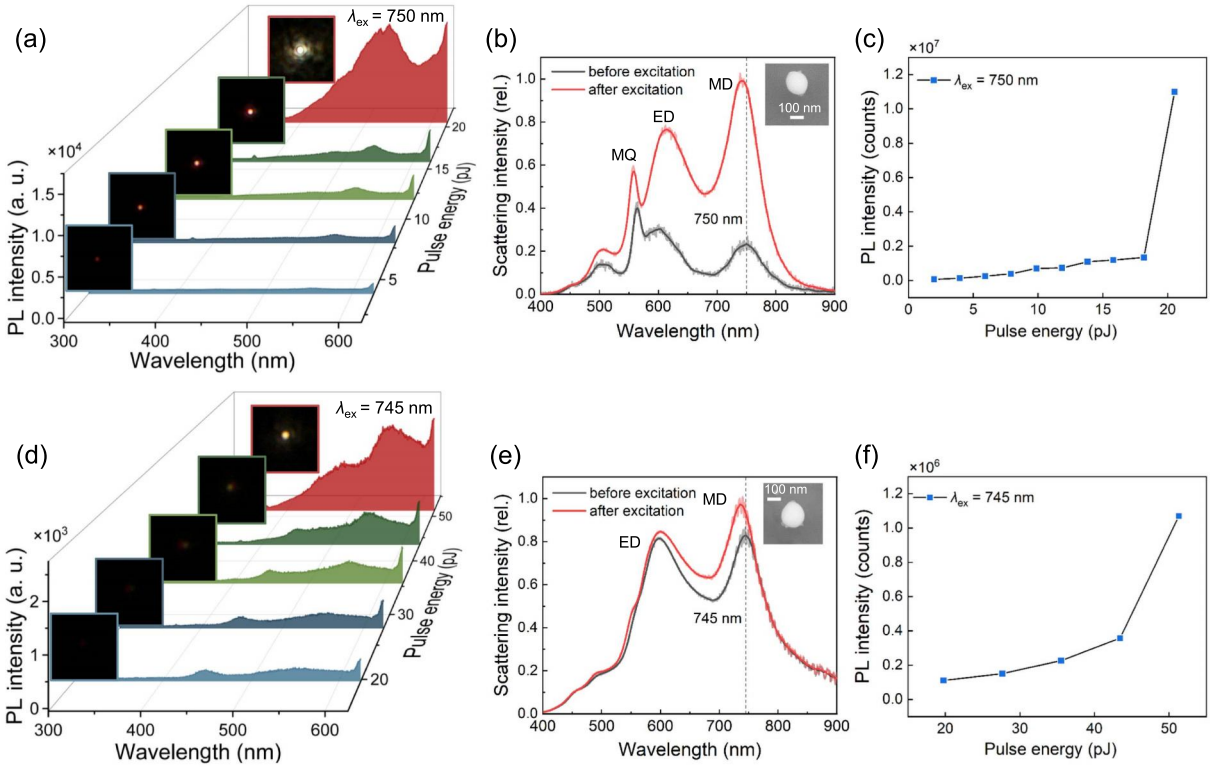

Fig. 3. Nonlinear optical emission from a $Si/Si_3N_4/Ag$ nanocavity under the excitation of femtosecond laser pulses. (a) PL spectra of the $Si/Si_3N_4/Ag$ nanocavity measured at different pumping pulse energies. The corresponding CCD images of the emission from the $Si/Si_3N_4/Ag$ nanocavity are shown in the insets. (b) Backward scattering spectra (normalized to the maximum value) measured for the $Si/Si_3N_4/Ag$ nanocavity before and after the luminescence burst. The scanning electron microscope (SEM) image of the Si nanoparticle before the excitation is shown in the inset. (c) Dependence of the integrated PL intensity on the pumping pulse energy observed for the $Si/Si_3N_4/Ag$ nanocavity. (d) PL spectra of a Si nanoparticle placed on a SiO_2 substrate measured at different pumping pulse energies. (e) Forward scattering spectra (normalized to the maximum value) measured for the Si nanoparticle placed on the SiO_2 substrate before and after the luminescence burst. (f) Dependence of the integrated PL intensity on the pumping pulse energy observed for the Si nanoparticle placed on the SiO_2 substrate.

The above results indicate clearly that the interaction between the Si nanoparticle and the femtosecond laser pulses can be effectively enhanced by the modified MD resonance supported by the $Si/Si_3N_4/Ag$ nanocavity, which possessed a larger Q factor. As a result, a low pulse energy threshold (~20.5 pJ) for the luminescence burst is achieved under the excitation of 750 nm femtosecond laser pulses. It should be emphasized that the generation of hot electrons in the conduction band is dominated by the 3PA process when the excitation wavelength is chosen at 750 nm. In this case, the threshold for the luminescence burst is larger than that reported in the previous study where the use of 720 nm femtosecond laser pulses implies that the 2PA and 3PA processes contribute simultaneously to the generation of hot electrons [28].

Recently, it was found that a Si_3N_4/Ag heterostructure can support TE waves with significantly reduced damping rates as compared with conventional surface plasmon polaritons (TM wave). More interestingly, the electric field of a TE wave is localized on the surface of the Si_3N_4 layer [31], which is beneficial for the interaction with a 2D material attached to the Si_3N_4/Ag heterostructure [33]. A further enhancement between the TE wave and the 2D material is expected if a Si nanoparticle is placed on the Si_3N_4/Ag heterostructure, forming a $Si/Si_3N_4/Ag$ nanocavity. In this case, the lateral confinement of the electric field in the $Si/Si_3N_4/Ag$ nanocavity leads to the electric field enhancement at the MD, ED, and MQ resonances supported by the nanocavity.

As shown schematically in Fig. 4(a), a $Si/Si_3N_4/Ag$ nanocavity is created by placing a Si nanoparticle on a Si_3N_4/Ag heterostructure. The nanocavity can be excited by the TE wave propagating on the surface of the Si_3N_4/Ag heterostructure stimulated by s-polarized incident light in the Kretschmann-Raether configuration [37]. In the experiment, we chose a Si nanoparticle with a diameter of $d \sim 190$ nm. The SEM image of the Si nanoparticle is shown in the inset of Fig. 4(b). We first examined the scattering spectrum of the $Si/Si_3N_4/Ag$ nanocavity under normal illumination, as shown in Fig. 4(b). We could identify the MQ, ED, and MD resonances supported by the $Si/Si_3N_4/Ag$ nanocavity, which appear at the wavelengths of ~530 nm, ~600 nm, and ~725 nm, respectively. Then, we examined the scattering of the $Si/Si_3N_4/Ag$ nanocavity excited by s-polarized light with different incident angles, which can generate TE waves on the surface of the Si_3N_4/Ag heterostructure. The scattering spectra of the $Si/Si_3N_4/Ag$ nanocavity measured at different incident angles are shown in Fig. 4(c). The actual incident angle θ at the SiO_2/Ag

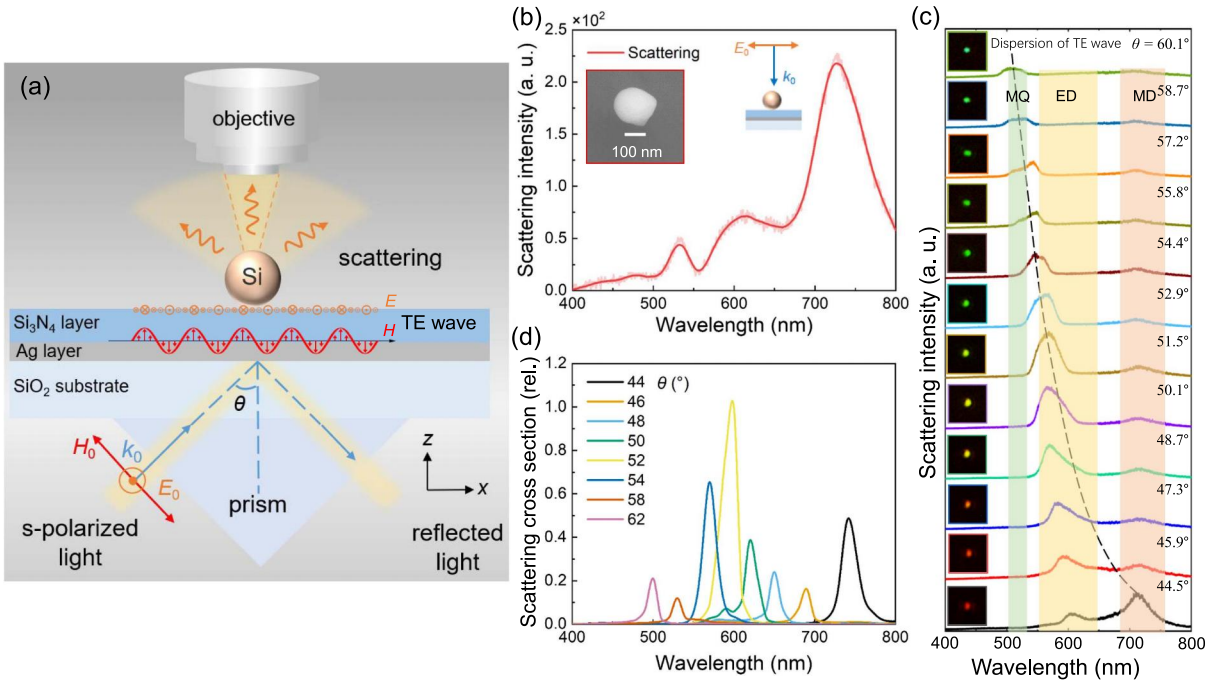

Fig. 4. Coupling between the TE wave supported by a Si_3N_4/Ag heterostructure and the Mie resonances supported by a Si nanoparticle in a Si/Si_3N_4/Ag nanocavity. (a) Schematic showing the excitation of a Si/Si_3N_4/Ag nanocavity by using the TE wave propagating on the surface of the Si_3N_4/Ag heterostructure stimulated by s-polarized incident light. The electric component (E) of TE wave is concentrated on the surface of the Si_3N_4 spacer, while the corresponding magnetic component (H) mainly exists at the Si_3N_4/Ag interface. (b) Backward scattering spectrum of the Si/Si_3N_4/Ag nanocavity. The SEM image of the Si nanoparticle is shown in the inset. (c) Measured scattering spectra of the Si/Si_3N_4/Ag nanocavity excited by s-polarized light with different incident angles. The corresponding CCD images of the scattering are shown in the insets. The wavelength bands where MQ, ED, and MD exist are denoted by green, yellow, and red shadows, respectively. The angular dispersion of the TE wave is represented by a dashed curve, schematically. (d) Simulated scattering spectra (in a relative scale) of the Si/Si_3N_4/Ag nanocavity excited by s-polarized light with different incident angles.

interface is calculated considering the refraction caused by the prism ($n_p \sim 1.5$) and the SiO_2 ($n_s \sim 1.46$) substrate. In each case, one can identify two scattering peaks in the scattering spectrum. One is fixed at ~725 nm while the other one has a blue shift with the increase of incident angle. It has been known that the wavelength of the TE wave decreases when the incident angle is increased. On the other hand, the Si nanoparticle supports three optical resonances located at ~530 nm. ~600 nm, and ~725 nm, corresponding to the MQ, ED, and MD resonances [denoted by shadows in Fig. 4(c)]. These two features are reflected in the scattering spectra of the Si/Si_3N_4/Ag nanocavity. The intensity of the TE wave is enhanced when its wavelength coincides with the optical resonances supported by the Si nanoparticle. The MD resonance can be found in all scattering spectra. However, its intensity is dramatically reduced at large incident angles when the wavelength of the TE wave is shifted to shorter wavelengths. It is expected that the electric field will be enhanced in the Si/Si_3N_4/Ag nanocavity due to the coupling between the TE wave and the Mie resonances.

In order to gain a deep insight into the scattering properties of the Si/Si_3N_4/Ag nanocavity, we calculated the scattering spectra of the Si/Si_3N_4/Ag nanocavity at different incident angles by using the FDTD method, as shown in Fig. 4(d). As the incident angle increases from 44° to 62°, the resonant wavelength of the TE wave has a blue shift from ~765 to ~500 nm. Remarkably, when the wavelength of TE wave overlaps with the intrinsic wavelength of the Mie resonances of the Si nanoparticle, scattering is enhanced and vice versa. The strongest scattering intensity is observed at ~600 nm, where the wavelength of the TE wave coincides with the ED resonance. It implies that the TE wave can be effectively coupled into the ED resonance. In the previous work, a polystyrene (PS) nanoparticle was used as the probe for the TE wave [33]; however, the intensity of the TE wave is only slightly modified due to the low refractive index of PS (see Appendix E). In contrast, the use of a high-index Si nanoparticle in this work can not only act as a probe but also achieve strong near-field enhancement. Therefore, the interaction between the TE wave and a 2D material will be enhanced in the Si/Si_3N_4/Ag nanocavity.

To verify the above expectation, we inserted a WS_2 monolayer into the Si/Si_3N_4/Ag nanocavity and examined the exciton-photon interaction, as schematically shown in Fig. 5(a). The SEM and forward scattering images of the Si/Si_3N_4/Ag nanocavities with an embedded WS_2 monolayer are shown in the insets. In the experiment, the region in which the spectrometer collects the scattering spectrum can be limited to ~1 μm^2 surrounding the Si nanoparticle, thus eliminating the influence of other scattered signals. We chose a Si nanoparticle with $d = 190$ nm and measured the angle-resolved scattering

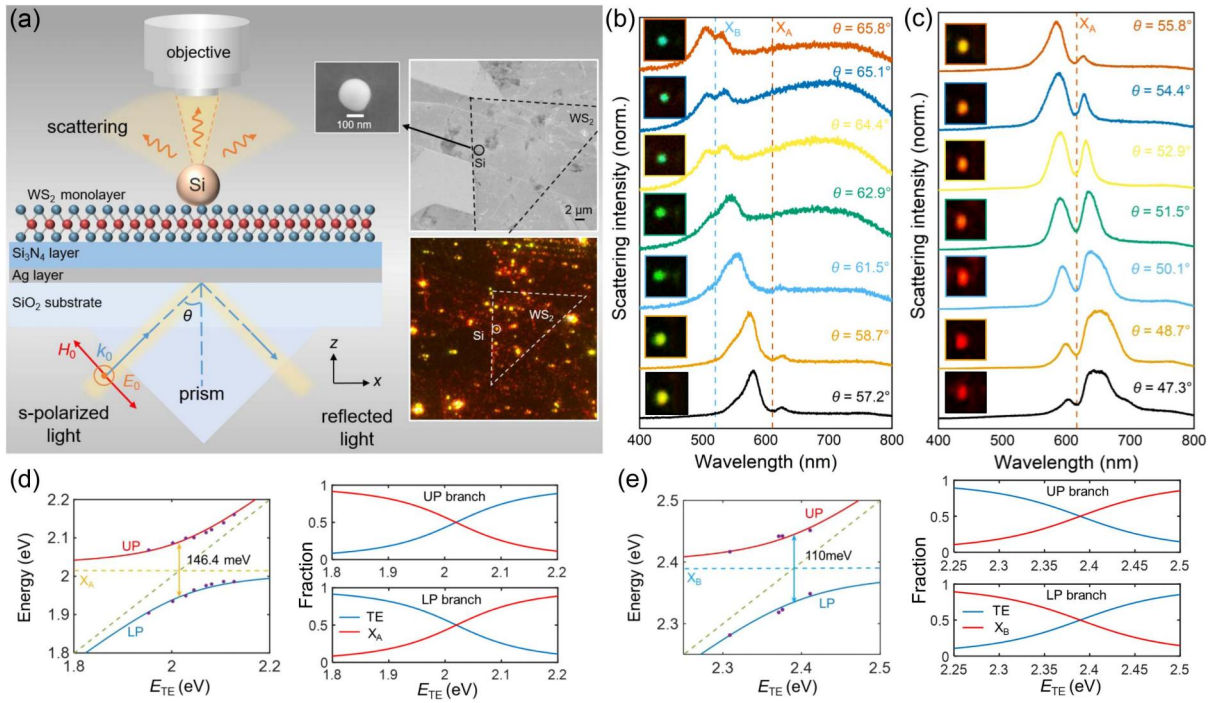

Fig. 5. Exciton-photon coupling in a $Si/Si_3N_4/Ag$ nanocavity with an embedded WS_2 monolayer. (a) Schematic showing the excitation of a $Si/Si_3N_4/Ag$ nanocavity with an embedded WS_2 monolayer and the detection of the scattered light. The SEM and forward scattering images of $Si/Si_3N_4/Ag$ nanocavities with an embedded WS_2 monolayer are shown in the insets. (b), (c) Angle-resolved scattering spectra of the $Si/Si_3N_4/Ag$ nanocavity ($d \sim 190$ nm) with an embedded WS_2 monolayer. Each of the spectra is normalized to its maximum value. The CCD images of the scattered light are shown in the insets. (d), (e) Dispersion relations of the upper and lower polariton branches (purple dots) extracted from the angle-resolved scattering spectra of the $Si/Si_3N_4/Ag$ nanocavity with an embedded WS_2 monolayer around the resonant wavelengths of the X_A and X_B. The red and blue curves are the fittings of the dispersion relations based on the coupled harmonic oscillator model. The energies of the excitons and photons (TE wave) are indicated by dashed lines.

spectra of the $Si/Si_3N_4/Ag$ nanocavity with an embedded WS_2 monolayer, as shown in Figs. 5(b) and 5(c). The CCD images of the scattered light are shown in the insets. By comparing the spectra with the results in Fig. 4(c), it can be found that the refractive index and material loss introduced by the WS_2 monolayer make the position of the resonant peak shift towards the longer wavelength at the same excitation angle. When the incident angle increased from 62.9° to 65.8°, a split of the scattering peak is observed, implying the coupling between the TE wave and X_B of the WS_2 monolayer. With the decreasing incident angle, the wavelength of the TE wave is shifted to longer wavelengths. Similarly, one can see a split of the scattering peak when the TE wave is moved to ~615 nm. It suggests the coupling between the TE wave and the X_A of the WS_2 monolayer.

Based on the angle-resolved scattering spectra measured for the $Si/Si_3N_4/Ag$ nanocavity with an embedded WS_2 monolayer, we could extract the dispersion relation of the lower and upper polaritons formed by the coupling between the TE wave and the two excitons of the WS_2 monolayer. The results for the X_A and X_B are shown in Figs. 5(d) and 5(e), respectively. The criterion for the strong coupling of optical mode and exciton is $E_R > \gamma_{TE} + \gamma_{ex}$, where E_R is the Rabi splitting energy, and γ_{TE} and γ_{ex} are the linewidths of the TE wave and exciton resonance, respectively [38,39]. Theoretically, the linewidths of A- and B-excitons can be derived from the imaginary part of the relative permittivity of the WS_2 monolayer [40]. In the analytical discussion, we use the theoretical linewidths of A- and B-excitons, which are 33 and 81 meV, respectively 33]]. The linewidths of the TE wave obtained from Fig. 4(d) are 91 and 65 meV, respectively, at the wavelengths of A- and B-excitons. As shown in Fig. 5(d), the Rabi splitting derived from the lower and upper polariton branches at the X_A was estimated to be ~146.4 meV, satisfying the strong coupling criterion. In addition, this value is larger than those observed in Si/Au nanocavities (~97 meV) [41] and $PS/Si_3N_4/Ag$ nanocavities (~130.1 meV) [33]. As discussed above, the intensity of the TE wave is greatly enhanced at ~600 nm by the ED resonance supported by the Si nanoparticle. Consequently, the in-plane electric field is enhanced due to the strong interaction between the TE wave and the ED resonance, leading to the enhanced exciton-photon coupling observed at the resonant wavelength of the X_A. Similarly, shown in Fig. 5(e), the Rabi splitting at the resonant wavelength of the X_B was derived to be ~110 meV from the fitting of the lower and upper polariton branches. The strong coupling condition is also fulfilled in this case. The corresponding simulation results are shown in Fig. 12 of Appendix F. The calculated Rabi splitting energy (~139.2 meV) for A-exciton agrees well with the measured value (~146.4 meV). However, the Rabi splitting energy obtained by simulation is ~227 meV, which is twice the measured one (~110 meV). By reviewing the results in Fig. 4(c), we can see that the scattering is very weak near

the wavelength of the B-exciton. At the same time, the radiation intensity of the B-exciton is much weaker than that of the A-exciton. These two reasons cause the scattered signal to be easily covered by the noise in the experiment. The signal noise caused by the divergence of the light source and the irregular shape of the Si nanoparticles also lead to the deviation of the experiment compared with the simulation results. In addition, a recent study revealed that the dissipation of coupled subsystems, such as optical modes and exciton, will cause the deviation between measured spectral splitting and theoretical eigenlevel splitting [42]. It enriches the understanding of strong light-matter interactions at room temperature.

3. CONCLUSION

In conclusion, based on $Si/Si_3N_4/Ag$ nanocavities, we investigated numerically and experimentally the enhanced interaction between femtosecond laser pulses and Si nanoparticles and that between a TE wave and a WS_2 monolayer. First, it was revealed that a $Si/Si_3N_4/Ag$ nanocavity can support an MD resonance with a larger Q factor than that supported by a Si nanoparticle placed on a SiO_2 substrate. By resonantly exciting the MD resonance of the $Si/Si_3N_4/Ag$ nanocavity with femtosecond laser pulses, we observed the luminescence burst from the Si nanoparticle with a threshold of ~20.5 pJ. Compared with a Si nanoparticle placed on a SiO_2 substrate, the threshold for the luminescence burst achieved in the $Si/Si_3N_4/Ag$ nanocavity is reduced by more than a half while the PL intensity is increased by one order of magnitude. Second, the coupling between the TE waves generated on the surface of the Si_3N_4/Ag heterostructure and the Mie resonances supported by the Si nanoparticle can effectively enhance the in-plane electric field, which leads to an enhanced exciton-photon coupling in a $Si/Si_3N_4/Ag$ nanocavity with an embedded WS_2 monolayer. Relying on the electric field enhancement achieved at the ED and MQ resonances of the $Si/Si_3N_4/Ag$ nanocavity, Rabi splitting energies as large as ~146.4 meV and ~110 meV were observed at the X_A and X_B of the WS_2 monolayer. It indicates an enhanced exciton-photon coupling at the X_A as compared with $PS/Si_3N_4/Ag$ nanocavities. The $Si/Si_3N_4/Ag$ hybrid nanocavity proposed in this work provides a useful platform for realizing the strong interaction of light with nanoparticles and 2D materials, which is beneficial for achieving nanoscale light sources.

APPENDIX A: MULTIPOLAR DECOMPOSITION

Multipolar decomposition is a key tool for analyzing the properties of resonant modes. Here, we adopt exact expressions for ED, MD, EQ, and MQ moments of dynamic sources. First, the electromagnetic field distributions of resonant modes in the $Si/Si_3N_4/Ag$ nanocavity excited by plane waves are calculated by using Ansys Lumerical based on the FDTD method. Then, the scattering cross section of multipolar moments is calculated by using the formulas proposed in Ref. [43], and the results are scaled by the surface area of the Si nanoparticle. Figure 6(a) shows the result of multipolar decomposition for the resonances excited by a plane wave with normal incidence. We can see that the resonant modes that exist around the wavelength of 600 nm and 765 nm are dominated by ED and MD, respectively.

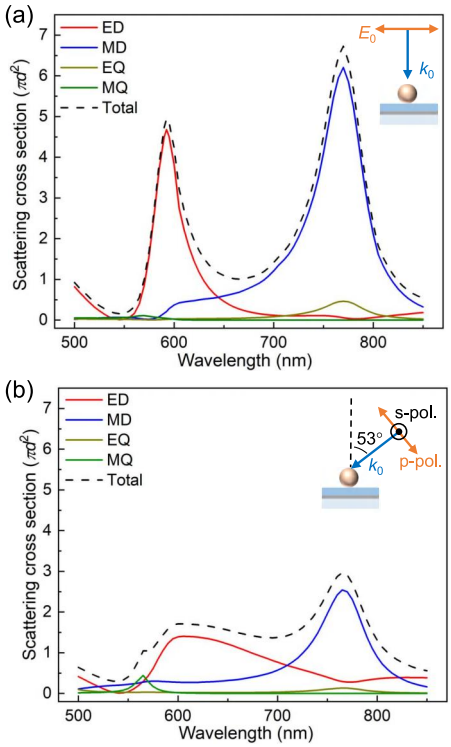

Fig. 6. Multipolar decomposition for resonances of the $Si/Si_3N_4/Ag$ nanocavity ($d = 195$ nm, $h_1 = 50$ nm $h_2 = 95$ nm). The dashed curve represents the sum of the scattering cross section of the four multipolar components. (a) The nanocavity is excited by a plane wave with normal incidence. (b) The nanocavity is excited by the simultaneous incidence of s-polarized and p-polarized plane waves with an incident angle of 53°.

The scattering cross section of EQ and MQ remains at very low levels throughout the whole spectrum. In addition, the large-angle components of the incident light produced by an objective (NA = 0.8) need to be considered. Figure 6(b) shows the result for the simultaneous incidence of s-polarized and p-polarized plane waves at the incident angle of 53°. Compared with the case of normal incidence, the spectra of ED and MD are broadened accompanied by decreased amplitude. Notably, the obliquely incident light can stimulate the MQ resonance at the wavelength of ~560 nm; this is consistent with the experimental result in Fig. 3(b).

APPENDIX B: SCATTERING SPECTRA OF HYBRID NANOCAVITIES COMPOSED OF SILVER FILMS WITH DIFFERENT THICKNESSES

Here, we numerically analyze the effect of the Ag layer on the resonance of the $Si/Si_3N_4/Ag$ nanocavity. Figure 7 shows the scattering spectra with different thicknesses (h_1) of the Ag layer. It can be seen that the scattering cross section at the wavelength of ~765 nm rises significantly when h_1 increases from 30 to 50 nm. When the thickness exceeds 50 nm, further increase in thickness has little effect on the scattering spectrum. It confirms that the 50 nm Ag layer is sufficient for the $Si/Si_3N_4/Ag$ nanocavity to support strong resonances.

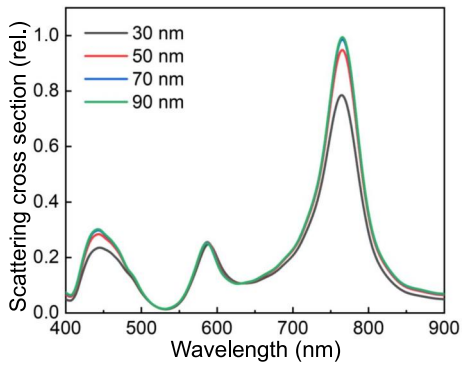

Fig. 7. Simulated scattering spectra (in a relative scale) of $Si/Si_3N_4/Ag$ nanocavities ($d = 195$ nm, $h_2 = 95$ nm) with different thicknesses of the Ag layer. The excitation light is a plane wave with normal incidence.

APPENDIX C: SCATTERING AND FIELD ENHANCEMENT OF THE Si NANOPARTICLE PLACED ON A SILICA SUBSTRATE

The simulated scattering and 2PA/3PA spectra of the Si nanoparticle placed on a SiO_2 substrate are shown in Fig. 8(a). It can be seen from the scattering spectrum that the strongest ED and MD resonances exist at the wavelengths of ~612 nm and ~741 nm, respectively. Although, the ED and MD resonances improve the enhancement factor of 2PA and 3PA, the peak values of the enhancement factor are far less than those of the $Si/Si_3N_4/Ag$ nanocavity. The main reason is that the ED and MD resonances with low Q factors supported by the Si nanoparticle placed on a SiO_2 substrate cannot generate

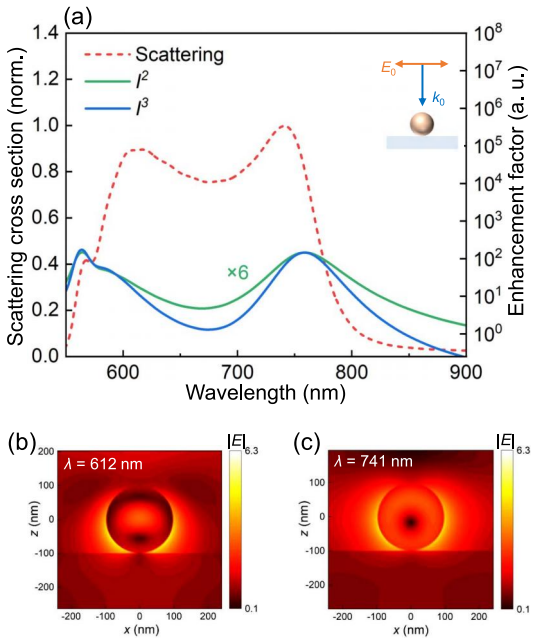

Fig. 8. Simulated results of the Si nanoparticle ($d = 195$ nm) placed on a SiO_2 substrate. (a) Scattering and 2PA/3PA spectra. The scattering spectrum is normalized to its maximum value. (b), (c) Electric field amplitude distributions at the ED and MD resonances.

strong field enhancements inside the Si nanoparticle. From Figs. 8(b) and 8(c), we can see that the strongest electric field intensity is on the surface of the nanoparticle rather than inside the nanoparticle. By comparing the results with the field distributions in Figs. 2(c) and 2(d), it can be found that the $Si/Si_3N_4/Ag$ nanocavity can significantly enhance the light intensity inside the Si nanoparticle.

APPENDIX D: NUMERICAL MODELING, SAMPLE FABRICATION, AND OPTICAL CHARACTERIZATION

1. Numerical Modeling

In this work, the scattering spectra and field intensity distributions of $Si/Si_3N_4/Ag$ hybrid nanocavities were calculated numerically by using Ansys Lumerical based on the FDTD method. In the simulation model, the Si nanoparticle was suspended 2 nm above the substrate surface to avoid point contact between the two geometries. The whole model adopted the four-level mesh accuracy built into Lumerical software. Within a cube region containing the Si nanoparticle, the mesh was further refined in three dimensions to a size of 2 nm. A total-field scattered-field (TFSF) source was used to solve scattering models. And, a perfectly matched layer boundary condition was employed to terminate the finite simulation region.

2. Sample Fabrication

Si nanoparticles with different diameters were fabricated by using femtosecond laser ablation. The 800 nm femtosecond laser pulses (Legend Elite, Coherent) with a duration of 90 fs and a repetition rate of 1 kHz were focused on the surface of a Si wafer immersed in deionized water using a lens with a focal length of 150 mm. The aqueous solution of Si nanoparticles was dropped onto the $Si_3N_4/Ag/SiO_2$ substrate and $WS_2/Si_3N_4/Ag/SiO_2$ substrate and allowed to dry naturally, obtaining the desired hybrid nanocavities.

The $WS_2/Si_3N_4/Ag$ heterostructure used in this work was fabricated by the following procedure. First, an Ag film with a thickness of 50 nm was plated on a SiO_2 substrate by using electron beam evaporation. Then, a WS_2/Si_3N_4 layer with a thickness of 95 nm was deposited on the Ag film through high-frequency plasma-enhanced chemical vapor deposition (HF-PECVD) to form a $WS_2/Si_3N_4/Ag$ heterostructure. The WS_2 monolayers purchased from Sixcarbon Tech Shenzhen were synthesized on a Si substrate via chemical vapor deposition and then transferred onto the Si_3N_4/Ag heterostructure, forming a $WS_2/Si_3N_4/Ag$ heterostructure.

3. Characterization of WS_2 Monolayer

Figure 9(a) shows the PL spectrum of the $WS_2/Si_3N_4/Ag$ sample under the excitation of a 488 nm laser with the power of 0.5 mW. A distinct single peak exists at the wavelength of ~615 nm corresponding to the direct excitonic transition for A-exciton; it rules out the possibility of multilayer WS_2 [44]. In addition, we also measured the Raman spectrum of the sample under the excitation of the 633 nm laser shown in Fig. 9(b). According to a previous work [45], spectral splitting exists at A_{1g} mode in the Raman spectra of two-layer and three-layer WS_2 samples. However, the measured Raman spectrum of our sample shows a clear single peak of A_{1g} mode at

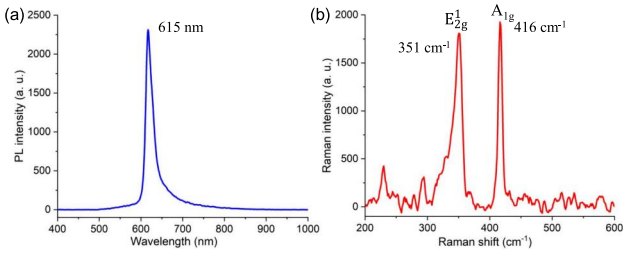

Fig. 9. (a) PL spectrum of the WS_2 sample placed on the Si_3N_4/Ag heterostructure using a 488 nm excitation laser with a power of 0.5 mW. (b) Raman spectrum of using a 633 nm excitation laser.

416 cm^{-1}. This result further proves that the sample used in our experiment is a WS_2 monolayer.

4. Optical Characterization

The experimental setups for measuring the nonlinear optical emission from the Si/Si_3N_4/Ag nanocavity under the excitation of femtosecond laser pulses are shown schematically in Fig. 10. The femtosecond laser pulses with a repetition rate of 76 MHz and a duration of 130 fs (Mira-HP) were used to excite Si nanoparticles placed on a Si_3N_4/Ag heterostructure. They were focused on Si nanoparticles by using a 100× objective lens (NA = 1.3) of an inverted microscope (Observer A1, Zeiss). The hot electron luminescence emitted from Si nanoparticles was collected by using the same objective lens and directed to a spectrometer (SR-500i, Andor) for analysis or a CCD (DS-Ri2, Nikon) for imaging.

The TE waves supported by the Si_3N_4/Ag heterostructure were excited in the Kretschmann-Raether configuration, as shown in Fig. 4(a). The sample was mounted on a prism made of SiO_2 (K9 glass) with silicone oil applied, which has a refractive index close to that of SiO_2. The TE wave was excited by utilizing the evanescent waves generated through total internal reflection at the surface of the prism. The scattering spectra of the hybrid nanocavities were characterized by using a dark-field optical microscope (Observer A1, Zeiss), with the choice of either broadband white light or s-polarized light for illumination.

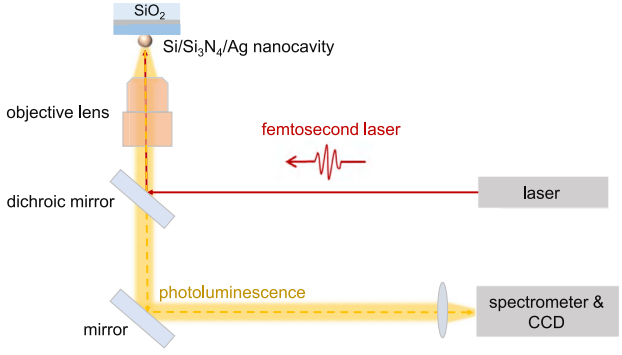

Fig. 10. Schematic diagram of experimental setups for measuring the nonlinear optical emission from the Si/Si_3N_4/Ag nanocavity under the excitation of femtosecond laser pulses.

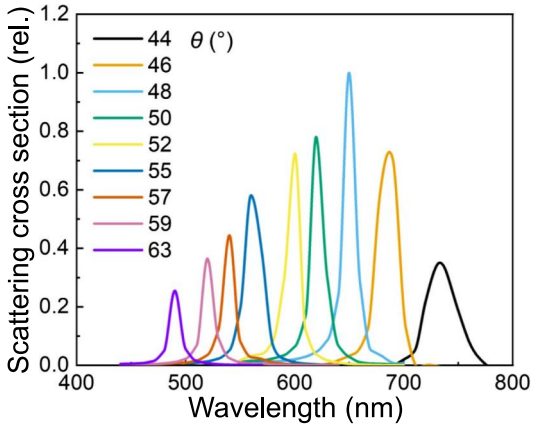

Fig. 11. Simulated scattering spectra (in a relative scale) of a PS nanoparticle (d = 300 nm) placed on the Si_3N_4/Ag heterostructure excited by s-polarized light in the Kretschmann-Raether configuration with different incident angles.

APPENDIX E: SCATTERING OF A POLYSTYRENE NANOPARTICLE PLACED ON THE HETEROSTRUCTURE

The refractive index of the PS nanoparticle (~1.59) is lower than that of the Si_3N_4 layer (~2.04). Thus, a PS nanoparticle placed on the Si_3N_4/Ag heterostructure cannot support resonances with high Q factors. When the TE wave supported by the Si_3N_4/Ag heterostructure meets the PS nanoparticle, it is only scattered by the PS nanoparticle without producing local field enhancement. Figure 11 shows the scattering spectra excited by s-polarized light with different incident angles. We can see that the peak wavelength of the scattered light has a blue shift with the increase of the incident angle. It is consistent with the dispersion characteristic of TE waves. In addition, the scattering peaks form a broad spectrum envelope, which indicates that the resonant modes supported by the PS nanoparticle have ultrahigh losses. Therefore, the PS nanoparticle can only act as a probe instead of being a nanocavity to achieve strong near-field enhancement.

APPENDIX F: SIMULATED SCATTERING SPECTRA OF THE HYBRID NANOCAVITY WITH AN EMBEDDED WS_2 MONOLAYER

Figure 12 shows the angle resolved scattering spectra of the Si/Si_3N_4/Ag nanocavity with an embedded WS_2 monolayer excited by s-polarized light when d = 190 nm. When the incident angle is ~50°, the resonant wavelength of the TE wave overlaps with the wavelength of A-exciton, which is consistent with the experimental result of ~51.5°. In addition, the measured Rabi splitting energy at the A-exciton (~146.4 meV) is very close to that obtained by simulation (~139.2 meV). For the coupling between the TE wave and B-exciton, the required incident angle in the experiment is around ~65.1°. However, this value is a bit larger than the angle (~61°) obtained in the simulation. The deviation in incident angle can be attributed to the divergence of an incident light beam. Especially, in the condition of large-angle oblique incidence, the TE wave interacting

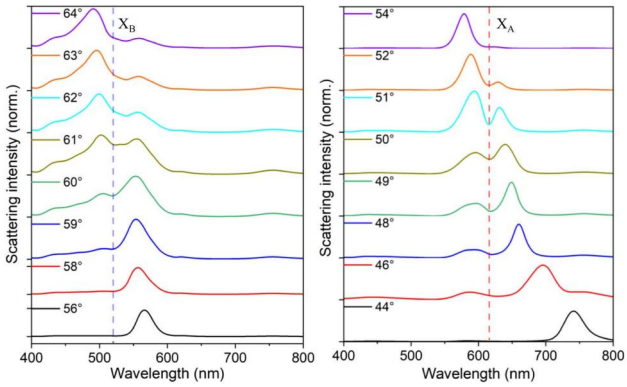

Fig. 12. Simulated angle resolved scattering spectra of the $Si/Si_3N_4/Ag$ nanocavity with an embedded WS_2 monolayer under the excitation of s-polarized plane wave.

with the Si nanoparticle is mainly excited by the edge of the light spot, which makes the deviation more obvious. Besides, since the resonance of B-exciton is much weaker than that of A-exciton, its measured scattering spectrum is easily affected by the non-collimated components of the incident light and the irregular structure of the silicon nanoparticle. Thus, the experimental Rabi splitting energy differs from the simulated results.

Funding. National Natural Science Foundation of China (12174123, 12374347); Basic and Applied Basic Research Foundation of Guangdong Province (2022A1515010747).

Disclosures. The authors declare no conflicts of interest.

Data Availability. Data underlying the results presented in this paper are not publicly available at this time but may be obtained from the authors upon reasonable request.

REFERENCES

1. A. I. Kuznetsov, A. E. Miroshnichenko, M. L. Brongersma, *et al.*, "Optically resonant dielectric nanostructures," Science **354**, aag2472 (2016).
2. G. Brönstrup, N. Jahr, C. Leiterer, *et al.*, "Optical properties of individual silicon nanowires for photonic devices," ACS Nano **4**, 7113–7122 (2010).
3. L. Cao, P. Fan, E. S. Barnard, *et al.*, "Tuning the color of silicon nanostructures," Nano Lett. **10**, 2649–2654 (2010).
4. K. Seo, M. Wober, P. Steinvurzel, *et al.*, "Multicolored vertical silicon nanowires," Nano Lett. **11**, 1851–1856 (2011).
5. A. B. Evlyukhin, S. M. Novikov, U. Zywietz, *et al.*, "Demonstration of magnetic dipole resonances of dielectric nanospheres in the visible region," Nano Lett. **12**, 3749–3755 (2012).
6. A. I. Kuznetsov, A. E. Miroshnichenko, Y. H. Fu, *et al.*, "Magnetic light," Sci. Rep. **2**, 492 (2012).
7. Y. H. Fu, A. I. Kuznetsov, A. E. Miroshnichenko, *et al.*, "Directional visible light scattering by silicon nanoparticles," Nat. Commun. **4**, 1527 (2013).
8. S. Person, M. Jain, Z. Lapin, *et al.*, "Demonstration of zero optical backscattering from single nanoparticles," Nano Lett. **13**, 1806–1809 (2013).
9. A. E. Krasnok, A. E. Miroshnichenko, P. A. Belov, *et al.*, "All-dielectric optical nanoantennas," Opt. Express **20**, 20599–20604 (2012).
10. A. E. Krasnok, C. R. Simovski, P. A. Belov, *et al.*, "Superdirective dielectric nanoantennas," Nanoscale **6**, 7354–7361 (2014).
11. A. E. Miroshnichenko, A. B. Evlyukhin, Y. F. Yu, *et al.*, "Nonradiating anapole modes in dielectric nanoparticles," Nat. Commun. **6**, 8069 (2015).
12. M. R. Shcherbakov, D. N. Neshev, B. Hopkins, *et al.*, "Enhanced third-harmonic generation in silicon nanoparticles driven by magnetic response," Nano Lett. **14**, 6488–6492 (2014).
13. M. R. Shcherbakov, P. P. Vabishchevich, A. S. Shorokhov, *et al.*, "Ultrafast all-optical switching with magnetic resonances in nonlinear dielectric nanostructures," Nano Lett. **15**, 6985–6990 (2015).
14. L. Shi, R. Fenollosa, T. U. Tuzer, *et al.*, "Angle-dependent quality factor of Mie resonances in silicon-colloid-based microcavities," ACS Photonics **1**, 408–412 (2014).
15. Y. Liang, K. Koshelev, F. Zhang, *et al.*, "Bound states in the continuum in anisotropic plasmonic metasurfaces," Nano Lett. **20**, 6351–6356 (2020).
16. Z. Wang, Y. Liang, J. Qu, *et al.*, "Plasmonic bound states in the continuum for unpolarized weak spatially coherent light," Photonics Res. **11**, 260–269 (2023).
17. Z. Liu, Y. Xu, Y. Lin, *et al.*, "High-*Q* quasibound states in the continuum for nonlinear metasurfaces," Phys. Rev. Lett. **123**, 253901 (2019).
18. L. Shi, E. Xifré-Pérez, F. G. de Abajo, *et al.*, "Looking through the mirror: optical microcavity-mirror image photonic interaction," Opt. Express **20**, 11247–11255 (2012).
19. E. Xifre-Perez, L. Shi, U. Tuzer, *et al.*, "Mirror-image-induced magnetic modes," ACS Nano **7**, 664–668 (2013).
20. I. Sinev, I. Iorsh, A. Bogdanov, *et al.*, "Polarization control over electric and magnetic dipole resonances of dielectric nanoparticles on metallic films," Laser Photonics Rev. **10**, 799–806 (2016).
21. Y.-C. Tseng, S.-W. Chang, Y.-C. Lee, *et al.*, "Cavity-enhanced magnetic dipole resonance induced hot luminescence from hundred-nanometer-sized silicon spheres," Nanophotonics **11**, 3583–3593 (2022).
22. Y. Liang, D. P. Tsai, and Y. Kivshar, "From local to nonlocal high-*Q* plasmonic metasurfaces," Phys. Rev. Lett. **133**, 053801 (2024).
23. I. Staude, T. Pertsch, and Y. S. Kivshar, "All-dielectric resonant metaoptics lightens up," ACS Photonics **6**, 802–814 (2019).
24. Z. Zhou, B. Yin, and J. Michel, "On-chip light sources for silicon photonics," Light Sci. Appl. **4**, e358 (2015).
25. L. Pavesi, L. Dal Negro, C. Mazzoleni, *et al.*, "Optical gain in silicon nanocrystals," Nature **408**, 440–444 (2000).
26. C. Zhang, Y. Xu, J. Liu, *et al.*, "Lighting up silicon nanoparticles with Mie resonances," Nat. Commun. **9**, 2964 (2018).
27. J. Xiang, S. Jiang, J. Chen, *et al.*, "Hot-electron intraband luminescence from GaAs nanospheres mediated by magnetic dipole resonances," Nano Lett. **17**, 4853–4859 (2017).
28. J. Xiang, M. Panmai, S. Bai, *et al.*, "Crystalline silicon white light sources driven by optical resonances," Nano Lett. **21**, 2397–2405 (2021).
29. M. Panmai, J. Xiang, S. Li, *et al.*, "Highly efficient nonlinear optical emission from a subwavelength crystalline silicon cuboid mediated by supercavity mode," Nat. Commun. **13**, 2749 (2022).
30. L. Zhou, M. Panmai, S. Li, *et al.*, "Lighting up Si nanoparticle arrays by exploiting the bound states in the continuum formed in a Si/Au hybrid nanostructure," ACS Photonics **9**, 2991–2999 (2022).
31. S. Li, L. Zhou, M. Panmai, *et al.*, "Magnetic plasmons induced in a dielectric-metal heterostructure by optical magnetism," Nanophotonics **10**, 2639–2649 (2021).
32. G. T. Papadakis, D. Fleischman, A. Davoyan, *et al.*, "Optical magnetism in planar metamaterial heterostructures," Nat. Commun. **9**, 296 (2018).
33. S. Li, L. Zhou, F. Deng, *et al.*, "Transverse-electric-polarized polaritons propagating in a $WS_2/Si_3N_4/Ag$ heterostructure," Laser Photonics Rev. **16**, 2100457 (2022).
34. W. De Boer, D. Timmerman, K. Dohnalova, *et al.*, "Red spectral shift and enhanced quantum efficiency in phonon-free photoluminescence from silicon nanocrystals," Nat. Nanotechnol. **5**, 878–884 (2010).
35. G. Yang, S. U. Dev, M. S. Allen, *et al.*, "Optical bound states in the continuum enabled by magnetic resonances coupled to a mirror," Nano Lett. **22**, 2001–2008 (2022).

36. Y. Mao, S. Bai, M. Panmai, *et al.*, "Controllable shaping of high-index dielectric nanoparticles by exploiting the giant optical force of femtosecond laser pulses," Photonics Res. **12**, 282–291 (2024).
37. E. Kretschmann, "Die Bestimmung optischer Konstanten von Metallen durch Anregung von Oberflächenplasmaschwingungen," Z. Phys. **241**, 313–324 (1971).
38. L. Hou, Q. Wang, H. Zhang, *et al.*, "Simultaneous control of plasmon–exciton and plasmon–trion couplings in an Au nanosphere and monolayer WS_2 hybrid system," APL Photonics **7**, 026107 (2022).
39. C. Li, H. Luo, L. Hou, *et al.*, "Giant photoluminescence enhancement of monolayer WSe_2 using a plasmonic nanocavity with on-demand resonance," Nano Lett. **24**, 5879–5885 (2024).
40. Y. Li, A. Chernikov, X. Zhang, *et al.*, "Measurement of the optical dielectric function of monolayer transition-metal dichalcogenides: MoS_2, $MoSe_2$, WS_2, and WSe_2," Phys. Rev. B **90**, 205422 (2014).
41. H. Huang, F. Deng, J. Xiang, *et al.*, "Plasmon-exciton coupling in dielectric-metal hybrid nanocavities with an embedded two-dimensional material," Appl. Surf. Sci. **542**, 148660 (2021).
42. J. Zhong, J.-Y. Li, J. Liu, *et al.*, "Room-temperature strong coupling of few-exciton in a monolayer WS_2 with plasmon and dispersion deviation," Nano Lett. **24**, 1579–1586 (2024).
43. R. Alaee, C. Rockstuhl, and I. Fernandez-Corbaton, "An electromagnetic multipole expansion beyond the long-wavelength approximation," Opt. Commun. **407**, 17–21 (2018).
44. T. Norden, C. Zhao, P. Zhang, *et al.*, "Giant valley splitting in monolayer WS_2 by magnetic proximity effect," Nat. Commun. **10**, 4163 (2019).
45. A. Barbosa, N. Figueroa, M. Giarola, *et al.*, "Straightforward identification of monolayer WS_2 structures by Raman spectroscopy," Mater. Chem. Phys. **243**, 122599 (2020).